

# A Direct Simulation Monte Carlo Study of the Environmental Conditions in Nanoscale Air Bearings Affecting Head Smear Formation

Roshan Mathew Tom<sup>1</sup>, David Bogy<sup>1</sup>

<sup>1</sup>Department of Mechanical Engineering, UC Berkeley, Berkeley, CA, 94720

## Abstract

We use the direct simulation Monte Carlo (DSMC) method along with the consistent Boltzmann algorithm to study the environmental factors affecting smear formation in a representative HAMR air bearing. We focus on the humidity, temperature, density, and velocity fields due to the high-temperature hotspot on the head-disk interface. We find that the gas temperature gradient in the vertical direction is significantly smaller than that expected by the temperature difference between the head and disk surfaces. This is possible since the head-disk clearance limits the mean-free path of the gas bearing. Consequently, the velocity field of the gas in the vertical direction also showed a drift from the colder to the hotter surface at low spacing. We also observed a high partial pressure of water vapor in the gas bearing, several times higher than the ambient level due to the higher gas temperature and pressure.

## Index Terms

Heat-Assisted Magnetic Recording, Smear, Head-Disk Interface, Air Bearing

## I. INTRODUCTION

**H**EAT-ASSISTED magnetic recording (HAMR) is the most promising technology to increase the areal density of hard disk drives [1]. This technology embeds a laser in the recording head that heats a nanoscale spot on the disk to reduce the magnetic media's coercivity while writing information before cooling down to freeze the data at room temperature. However, a large temperature gradient, accompanied by an electric field gradient, can cause premature failure of these heads. Therefore, it is critical to design a robust head-disk interface for the long-term success of HAMR. Several experiments conducted at the head-disk interface reveal the presence of contaminations on the surfaces of the head and disk [2, 3]. These contaminations appear to be smeared on the surfaces and are commonly called "smear." They are formed from several sources, such as the PFPE lubricant, disk materials, and airborne contaminants such as silica. An atomic force microscope (AFM) image of smear is shown in Fig. 1. The air-bearing that supports the slider to maintain a steady head-disk spacing can be as thin as 1 nm. Therefore, smear can cause significant instabilities in the sliders' flying characteristics, eventually leading to a head crash on the disk. Mitigating smear is key for reliable HAMR drives, and it has seen considerable research attention [4–10].

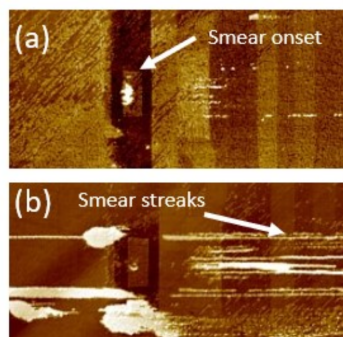


Fig. 1. AFM Image of smear from ref. [5]

A critical step in studying smear is to understand its formation and the factors that influence its growth. Several mechanisms have been proposed [4, 5, 11, 12]. The temperature gradient has received the most attention. However, other forces, such as optical forces, have also been studied. Due to the multi-dimensional nature of smear, including its diverse composition, it is likely that several mechanisms act concurrently to influence the onset and growth of smear. The region where the smear

grows, the head-disk interface, extends several micrometers in the down-track and cross-track directions, but it is only several nanometers in the vertical direction. This raises the important question of whether to model the surfaces and smear as a continuum solid/fluid or as atoms and molecules. Each approach has its advantages and disadvantages. However, both have been used to expand our understanding of smear formation and mitigation [5, 13, 14]. Arguably, each model would inform the other to create a robust simulation strategy that can capture all aspects of smear.

The minimum thickness of the air bearing can be as low as 1 nm, which is only the size of three to four helium atoms. However, the air-bearing modeling and design primarily use a thin-film continuum theory [15]. Nevertheless, a particle-based study showed that continuum theory yields similar results when calculating the bearing forces on the slider [16]. However, air-bearing in HAMR introduces new conditions, such as the temperature hotspot. Given that the primary medium of smear transport is the air-bearing, the characteristics of the air-bearing under this temperature field need to be investigated. In this report, we look into the temperature, density, and velocity fields in a representative HAMR gas bearing.

Humidity is also crucial for the reliability of HAMR. It has been shown to induce a water monolayer on the disk surface [17, 18], decrease the tribocharge in the slider-disk interface [19], influence the lubricant transfer between the head and the disk [20], enhance the heat transfer between the protrusions from the head in contact with the disk when the RH is greater than 75% [21], affect the spreading rate and chemisorption of the lubricants on the disk surface [22], reduce the vaporization energy and thus increase evaporation of lubricants during thermal desorption [23, 24], and promote corrosion of the recording layers [25]. These results show a clear relationship between humidity and the reliability of hard disk drives. Therefore, we also consider the behavior of water molecules in the air-bearing.

The organization of this paper is as follows. In Section II, we begin by describing the model used to simulate the air-bearing. We use a particle-based method, Direct Simulation Monte Carlo (DSMC), with a dense gas modification. Further, we explain the simulation conditions, specifically the approximation of the head-disk interface. We then present the results of our simulation in Section III. Finally, in Section IV, we present the conclusions and the scope for further study.

## II. NUMERICAL MODEL

### A. Simulation method

The molecular gas lubrication (MGL) theory, along with the Fukui-Kaneko slip correction, is the accepted method for calculating the properties of the gas bearings in the head-disk interface [15]. However, it does not give insight into the molecular nature of the gas-bearing. Since the minimum head-disk clearance in recent hard drives is around 1 nm, the particle nature of the air-bearing can have a significant impact on the movement of contaminants in the head-disk interface. In this study, we use a particle-based method, Direct Simulation Monte Carlo (DSMC), to study the air bearings of HAMR head-disk interface.

The DSMC method solves the Boltzmann Transport Equation by tracking the trajectory of individual particles (atoms and molecules) in the simulation domain [26]. Statistical averages are then taken to extract macroscopic properties. Unlike a molecular dynamics (MD) simulation, it employs the use of stochastic functions to calculate the collision, position, and velocity of the particles [27]. The method begins by using simulated particles that are statistical equivalents of real particles. If each real particle can be located by its position and velocity,  $\{\mathbf{x}, \mathbf{v}\}$ , then all real particles within the space  $\{\mathbf{x} + d\mathbf{x}, \mathbf{v} + d\mathbf{v}\}$  are represented by one simulated particle. The positions, velocities distribution, and collisions of the DSMC particles are chosen to match that of real particles. The ratio between the simulated and real particles is a global input to the solver. The initial velocity distribution is governed by the Maxwell-Boltzmann distribution given by,

$$f(\mathbf{v}) = \left[ \frac{m}{2\pi k_B T} \right]^{3/2} \exp\left(-\frac{m\mathbf{v}^2}{2k_B T}\right) \quad (1)$$

where  $m$ ,  $k_B$ ,  $T$ , and  $v$  are the particle mass, the Boltzmann constant, the local temperature, and the particle velocity. At each timestep, the collisions and movements of the particles are decoupled. First, each particle is advected along its velocity by Newtonian mechanics. Then, collisions between particles are calculated. In physical fluids, two particles that are separated by a distance greater than their mean free path rarely collide. Therefore, DSMC divides the domain into discrete cells that are roughly the mean free path of the particles [28]. The timestep is taken to be less than the relaxation time. Collisions are then conducted within each cell according to the properties of the particles contained within it. Various collision models can be used, such as the hard sphere [26], variable hard sphere [29], variable soft sphere [30], and the generalized hard sphere model [31]. The simple sphere model considers particles as rigid spheres with diameter,  $d$ . The scattering angle, which is the deflection of the particle on collision is given by,

$$\chi = 2 \cos^{-1} \left( \frac{b}{d} \right) \quad (2)$$

where  $b$  is the impact parameter. This study uses the variable soft sphere (VSS) model of Koura and Matsumoto [30] that introduces two modifications to the hard-sphere model. First, the diameter changes with the temperature of the gas, given by:

$$d_{eff} = d_0 \left( \frac{T}{T_0} \right)^\omega \quad (3)$$

where  $d_0$  and  $T_0$  are the reference diameter and temperature of the gas,  $T$  is the current temperature of the grid cell, and  $\omega$  is a temperature-dependent viscosity term. The scattering angle,  $\chi$  is then modified by the angular scattering term,  $\alpha$ , as,

$$\chi = 2 \cos^{-1} \left( \frac{b}{d} \right)^{1/\alpha} \quad (4)$$

The parameters  $d_0$ ,  $T_0$ ,  $\omega$ , and  $\alpha$  are derived from experiments or more sophisticated models. We used the parameters from Ref. [32] as listed in Table I.

Gas	Molecular Mass ( $\times 10^{-26}$ kg)	$d_0$ (nm)	$\omega$	$T_0$ (K)	$\alpha$
Nitrogen	4.6495	0.3871	0.686	353.15	1.365
Helium	0.6642	0.2298	0.712	350.00	1.429

TABLE I  
COLLISION PROPERTIES OF THE AIR BEARING FROM REF. [32]

The DSMC method has been used to test the MGL theory on gas bearings in HAMR head-disk interfaces [33, 34]. The bearing force predicted by MGL and DSMC was within 4% of each other [16]. The DSMC method was initially developed for rarefied gas flows, so the particles are considered point masses [35]. However, in dense gases, such as those in the gas bearings of hard disk drives, the particles' inter-atomic forces and finite sizes can influence their behavior [36]. The consistent Boltzmann algorithm (CBA) was developed to account for the finite volume of the particles [37]. First, the number of collisions in each cell was increased by a "Y-factor", which accounted for the reduced volume available for particle movement. The Y-factor is given by [38]

$$Y = \frac{1 + 0.0555678\zeta n + 0.013944551\zeta^2 n^2 - 0.0013396\zeta^3 n^3}{1 - 0.56943218\zeta + 0.08289011\zeta^2 n^2} \quad (5)$$

where  $\zeta = \frac{2}{3}\pi\sigma^3$ ,  $\sigma$  is the collision diameter and  $n$  is the number density. Further, the particles that collided had their positions advected by an additional displacement. The need for this extra displacement is illustrated in Fig. 2.

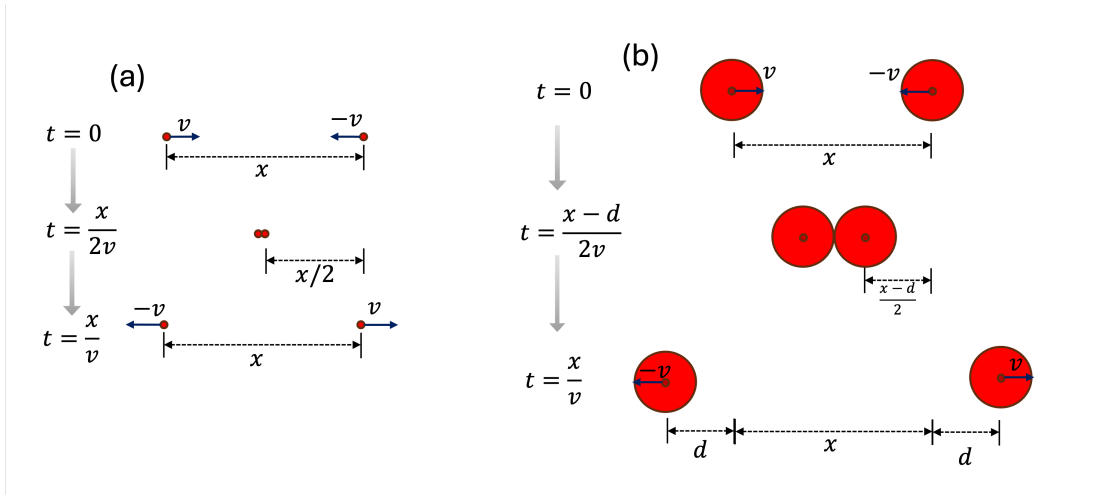


Fig. 2. Schematic to illustrate the need for CBA. (a) is the case when the particles are point masses. (b) is the case when the particles have a finite diameter

On the left side (Fig. 2a), we track the trajectory of two particles (red dots) separated by a distance  $x$  and moving towards each other with speed  $v$ . As these particles are assumed to be point particles, at  $t = x/2v$ , the particles collide and change the direction of travel. Then, at  $t = x/v$ , they return to their initial positions, which are  $x$  units away. Then, Fig. 2b shows the collision of the same particles but with a diameter,  $d$ . Since they possess a finite diameter, the center-to-center distance between the two particles is equal to  $d$  at impact. Therefore, the collision occurs at  $t = \frac{x-d}{2v}$ . Then, after the collision, they retrace their path. However, at  $t = x/v$ , the final positions are separated by a distance  $d$  from their initial position. This extra

displacement needs to be accounted for by the following equation,

$$\mathbf{d}_{cba} = \frac{\mathbf{v}'_r - \mathbf{v}_r}{|\mathbf{v}'_r - \mathbf{v}_r|} \sigma \quad (6)$$

where  $v_r$  and  $v'_r$  are the particles' pre and post-collision relative velocities. We ignore the inter-atomic forces in the study. When replicating the simulation conditions from Huang (1997) [16], we observe a 2% higher bearing force after applying CBA. Therefore, this effect may be one source of the minor difference between the MGL and traditional DSMC models.

The DSMC method has been proven to converge to the Boltzmann equation [39], has been thoroughly tested in high Knudsen-number flows [27], and excellent agreement has been found with experiments [40]. Due to the relative simplicity of setting up a DSMC simulation and the ability to study gas mixtures, we use the modified DSMC method to study the air-bearing [41]. We modified the open-source software SPARTA [42] to run all DSMC simulations in this study.

### B. Simulation conditions

A typical hard drive slider is hundreds of microns in size, with special etchings on the air-bearing surface to produce the precise bearing force required to counter the head suspension load. The ABS designs used in HAMR drives are not public. Moreover, modeling such a large system would be too computationally expensive in terms of power and memory requirements. Therefore, we use a model of the local thermal fly-height protrusion that can capture the necessary details of the HAMR head-disk interface for our analysis. As shown in Fig 3a, a channel with varying cross-sections is used. The protrusion-like feature in the schematic is relatively long to capture various phenomena clearly, whereas, in real HAMR heads, the protrusion is localized near the NFT and read/write elements. The top surface represents the head with a peak temperature of 500 K. The bottom surface represents the disk with a peak temperature of 800 K. The temperature distribution along the channel is shown in Fig. 3b. The temperature gradient along the downtrack direction reaches up to 1 K/nm. The peak temperature is held fixed for several hundred nanometers to reduce any measurement noise while calculating macro properties such as pressure or temperature. The main difference between an actual HAMR head and our model is that the peak temperatures are formed over a small region, typically a few tens of nanometers wide.

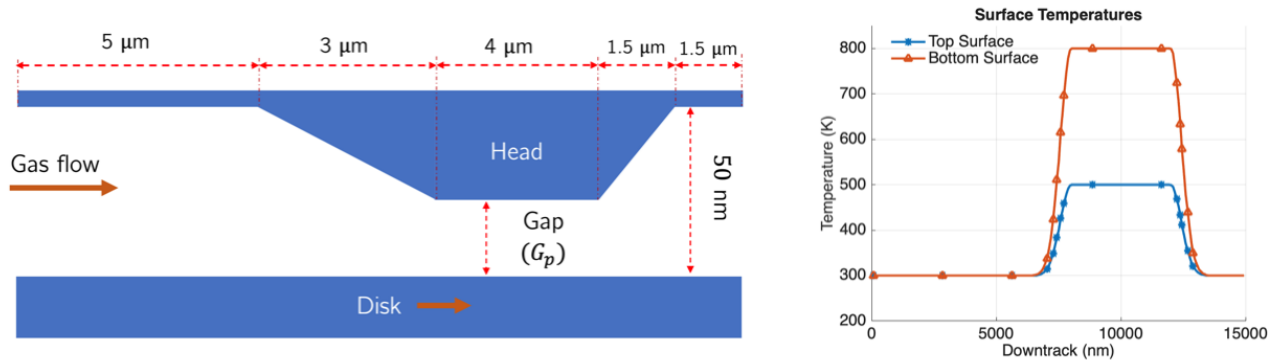


Fig. 3. (a) Schematic view of the head-disk interface and (b) Temperature distributions

The disk moves at a constant velocity of 50 m/s in the downtrack direction. Both surfaces behave like solid walls that reflect or reset the incident particle's velocity with a given accommodation factor, usually represented by  $\alpha$ . The velocity reset occurs according to a Maxwellian velocity distribution. This study assumes a perfect accommodation factor of 1. Further, along the down-track direction, there is an inflow and outflow boundary condition, where particles are inserted or removed to maintain atmospheric pressure at both boundaries. The cross-section is designed to allow for smooth airflow near the inlet boundary [43]. The channel dimensions are 15  $\mu\text{m}$  in the down-track direction and 50 nm in the vertical direction. The channel width (into the plane) is assumed to be infinite, with periodic boundary conditions being enforced.

The dimension of a DSMC cell must be less than the mean free path of the gas particles so that all particles in each cell can physically collide. However, very small cell sizes would increase the computational costs. Since the mean free path depends on the temperature and pressure, we adapt the cell size to the local temperature and pressure. The maximum cell size was set to be 25 nm and the smallest was 1 nm. The chosen timestep should also be smaller than the mean collision time. From kinetic theory, the mean collision time is between 29 to 41 ps (picosecond) for the temperature and pressure ranges we countered. Thus, we used a conservative timestep of 10 ps for the rest of the simulation. We also allowed each simulation to reach equilibrium by running for about 150,000 steps before any measurements were made.

To simulate humidity, we considered water vapor molecules to be a separate gas. Each water molecule was approximated as a hard sphere with an effective diameter of 270 pm. The inlet and outlet boundaries were set at 20% relative humidity

( $\approx 700$  Pa) pressure. As the temperature on the disk (800 K) exceeds the critical temperature of water, condensation would not occur on the disk surface. On the head surface (500 K), the water saturation pressure is around 25 atm, much greater than the expected partial pressure of water vapor, leading to negligible condensation. Therefore, water condensation on the head surface could be ignored.

### III. RESULTS

#### A. Pressure

We simulated a range of gaps, from 1 nm to 25 nm for both nitrogen and helium bearings. The top and bottom surfaces were divided into 2000 surface elements, and the pressure on each element was calculated by summing over the momentum change of incident molecules per unit time. The pressures over 400,000 timesteps were averaged to obtain uniform results.

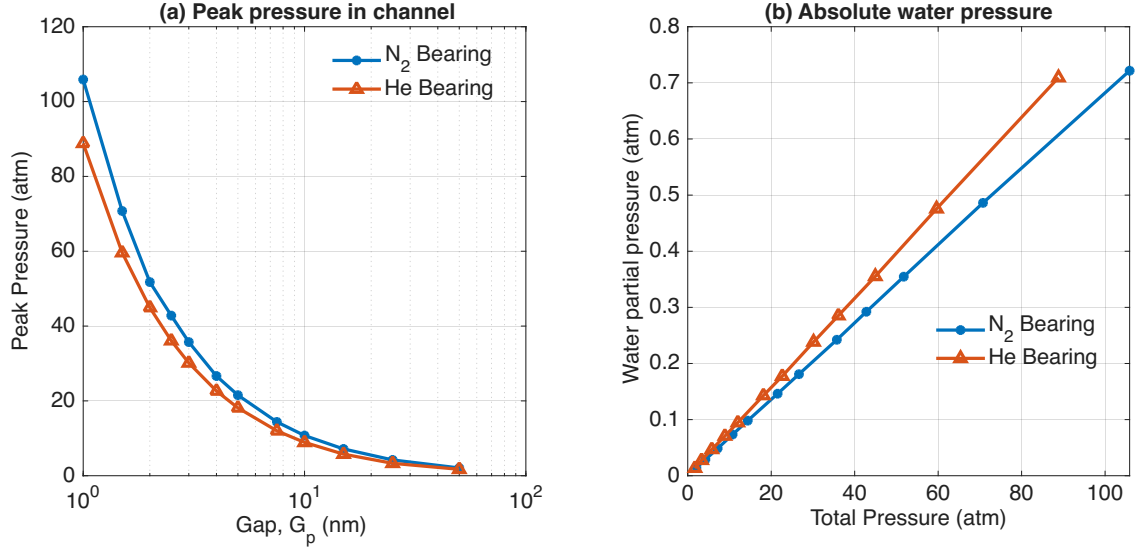


Fig. 4. (a) Peak pressure in the channel with hotspot, (b) Partial pressure of water at various total pressures

Fig. 4a shows the pressure as a function of the minimum spacing. With decreasing spacing, the total pressure exponentially increases to exceed 80 atm at one-nanometer spacing. At this spacing, nitrogen and helium bearings show up to an 18 atm pressure difference ( $> 20\%$ ) as the non-ideal gas effects play a larger role. Nitrogen, being a larger molecule, exerts a higher pressure as expected from Eq. 6. However, as the spacing increases, the difference gradually reduces as the non-ideal gas effects become insignificant.

We also look at the partial pressure of water vapor as plotted in Fig. 4b against the peak gas bearing pressure. The partial pressure linearly increases with the gas-bearing pressure (which from Fig. 4a increases with decreasing spacing). The mechanism that compresses the gas also compresses the water vapor. Therefore, the slope is also roughly equal to the ratio of partial pressures at the inlet (0.007). At room temperature the saturation pressure of water is around 3 kPa, however, the gas channel has a water vapor partial pressure of 70 kPa. This is possible as the high head and media temperatures raise the saturation pressure significantly to prevent any condensation. We also observe a slight difference between the water content in nitrogen and helium. Nitrogen being the larger molecule, displaces some of the water molecules resulting in 10-15% lower water pressure. The actual pressure in HAMR operations depends on ambient humidity and the evaporation from the head and disk surfaces.

To investigate further, we plot the total pressure distribution on the head and disk surfaces in Fig. 5. The pressure is 1 atmosphere at the inlet, then rises rapidly to a steady value for both gas bearings. The steady pressure is maintained throughout the thinnest region before dropping immediately. The region of steady pressure is unique to our design as the gap region in Fig. 3 is relatively long. In actual HAMR drives, the peak pressure would be more localized. Nevertheless, for the purposes of this study, the elongated pressure allows us to study the localized region better.

We also see that the pressure distributions on both the disk and head surfaces are identical for helium (green and purple lines) and nitrogen (blue and red lines). This must happen as any pressure gradient would lead to a flux of particles in the vertical direction to equalize this pressure. However, since the temperatures at the two surfaces differ by 300 K, the other properties of the gas-bearing at the two surfaces should also be different to maintain equal pressure. As a consequence of the non-ideal gas equation (Eq. 7), the pressure depends on three quantities - the number density, temperature, and the correction term to account for non-ideal effects.

$$P = nkT(1 + \phi) \quad (7)$$

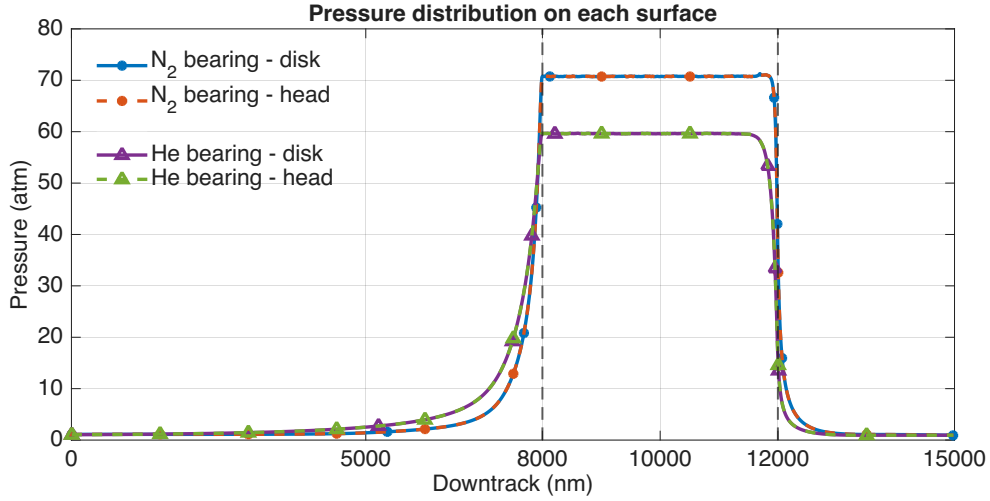


Fig. 5. Pressure distribution along the top and bottom surface for helium and nitrogen bearings at 1.5 nm gap

where,  $P$ ,  $n$ ,  $k$ ,  $T$ , are the pressure, number density, Boltzmann constant, and temperature, respectively. In our case, the correction term ( $\phi$ ) is a function of the diameter of the particle (Eq. 6). Since the particle's properties are constant throughout the simulations, the gas temperature and number density are the only candidates that account for the constant pressure, which we will examine next.

### B. Density and Temperature

Temperature and number density are defined as the average energy and number of molecules over a unit volume, respectively. Therefore, when the head-disk spacing is in the order of a nanometer, they cannot be defined at any number of arbitrary points along the vertical direction, but only over discrete volumes that approach the molecules' size. Therefore, we restrict the calculation of the density and temperature to the grid cell adjacent to each surface element. The adaptive grid cell size algorithm ensures that the dimension of the cell does not exceed the mean free path of a gas particle. Fig. 6 shows the nitrogen bearings' number density and temperature distribution for a 4 nm spacing. The solid lines mark the quantity along the disk surface, and the dashed lines mark the quantity along the head surface. They show that the temperature and number density profiles follow different distributions at the head and disk surfaces near the hotspot. This ensures that the pressure is equal even if the surface temperatures differ. Fig. 7a, shows the differences in number density at the top and bottom surface over a range of gaps. As the spacing decreases, the density difference between the two surfaces also increases. This increase can be correlated with absolute pressure increase found at lower spacings.

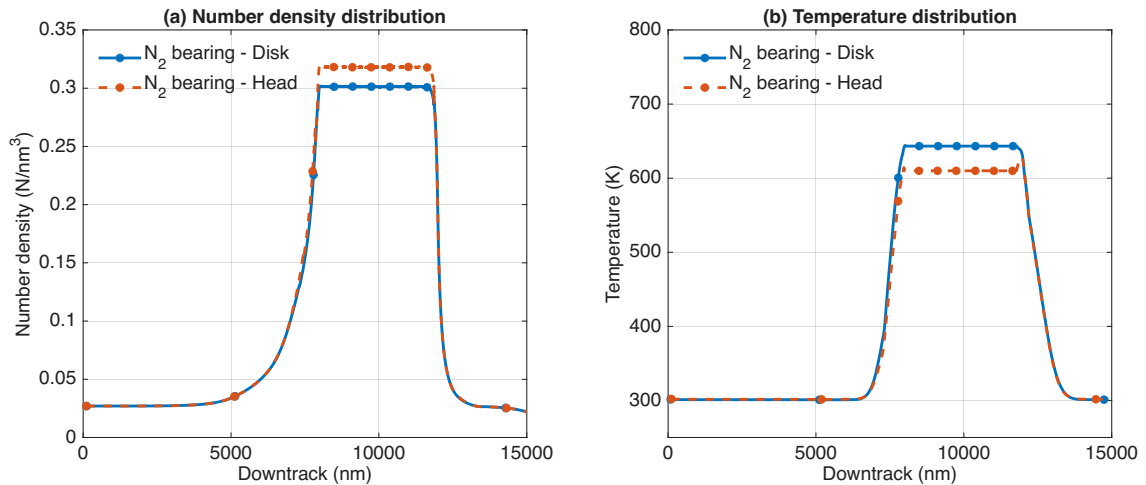


Fig. 6. (a) Number density distribution along the head (top) and disk (bottom) surfaces for nitrogen-bearing with 4 nm gap (b) Temperature distribution along the head (top) and disk (bottom) surfaces for nitrogen-bearing with 4 nm gap

Further, Fig. 7b shows the temperature difference between the head and disk surfaces. We observe a small 20 to 40 Kelvin temperature difference between the two surfaces, with a higher gas temperature at the disk surface. This stands in contrast to

the difference in the head and disk surface temperatures temperature difference of 300 K. The gas temperature near the surface is not equal to the surface temperatures, rather there is a temperature jump between the surface and the gas. This is related to Kapitza resistance, which was first measured in the interface between superfluid helium and a solid [44]. These temperature jumps are also found in other interfaces and various theories to their origins have been proposed [45].

The mechanism behind this observation can be understood when we look at the history of the atoms at any point. The gas atoms just above the disk surface are primarily from two sources. On the one hand, we have those particles that are just reflected from the disk surface with energies corresponding to 800 K. On the other hand, we have particles coming from the head surface. Because of the scarce intermolecular collisions, these atoms do not lose or gain energies apart from that which they received from the head. Therefore, they have energies corresponding to 500 K. The net effect is that the temperature in the gas bearing is the average of the head and disk temperatures (650 K). Further, because the atoms from the head are slower than those from the disk, at any given time, there are more particles from the head in the interface with temperatures slightly lower than 650 K.

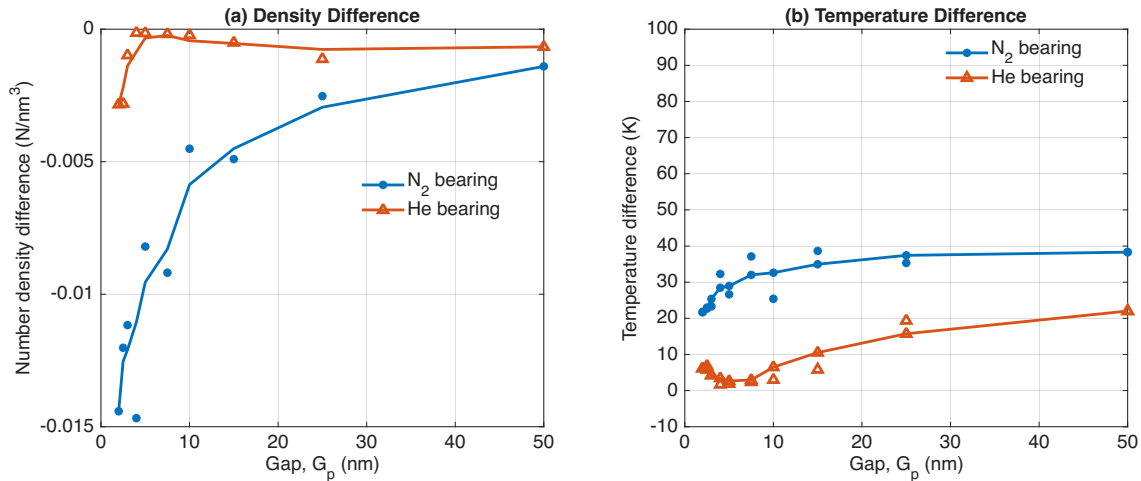


Fig. 7. (a) The average difference in the number density for gas bearings at different gap values (b) The average temperature difference for gas bearings at different gap values. Each data point is the value at the disk (bottom) surface subtracted from the corresponding value at the head (top) surface.

### C. Vertical drift

As particles bounce off the surfaces, the diffusive boundary condition at the surfaces ensures that the kinetic energy of the particles corresponds to the surface temperature. Consequently, the particles bouncing off the hotter side have, on average, higher velocity than those from the cooler side. As a result, at any given time, more particles travel from the head to the disk surface than the other way around. The net effect is a vertical drift from the top to the bottom. We can observe this in Fig. 8, where we plot the vertical component of the velocity along the down-track direction. There is also a small overshoot at the rear end (at  $\approx 12500$  nm downtrack) with a positive drift of 0.5 m/s. This is also the location where the channel broadens out. As a particle exits from the thinnest region, it moves up to occupy the empty space, and a positive overshoot is formed.

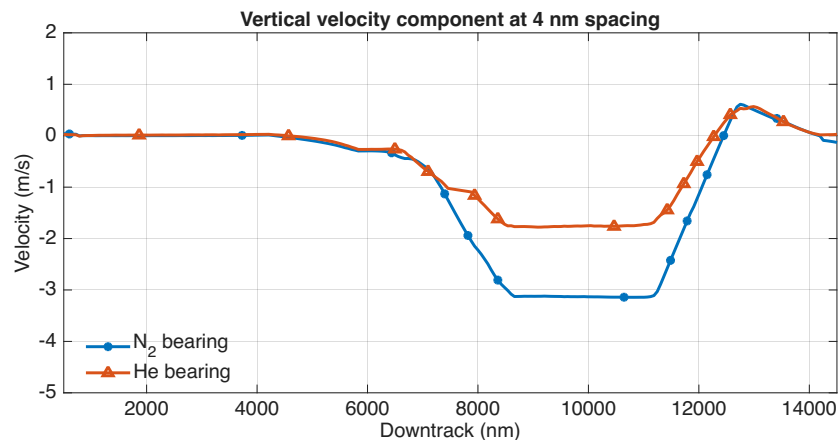


Fig. 8. The vertical component of the gas velocity for nitrogen and helium bearings at 4 nm gap

#### D. Collisions in the head-disk interface

If we count the collisions in the gap, we can confirm the presence of the ballistic trajectory where the head and disk surfaces are closest. Consider the two kinds of collisions - intermolecular collisions between gas molecules and surface collisions between gas molecules and surfaces. We counted each type of collision at the gap and plotted them in Fig. 9. The intermolecular collisions decrease with clearance as the pressure drop dominates. The surface collisions also decrease with spacing as the pressure exerted by the air-bearing reduces, causing fewer particles to hit each surface. We define the collision ratio as the number of surface collisions for every intermolecular collision. For each gap, the collision ratio is always greater than 1. This indicates that each gas particle collides with other particles after several surface collisions. This suggests they follow a ballistic trajectory (rarefied flow) in these spacings despite pressures exceeding 50 atm, and the head disk clearance limits the mean free path. In other words, this regime resembles rarefied gas dynamics. Helium and nitrogen exhibit different collision ratios due to their molecule's sizes and masses. The faster helium atoms collide with the surface at a faster rate than the slower nitrogen molecules. We note that the trends for the collision ratio would vary with the channel design as seen in Ref. [41]. The rarefied flow has several implications for the reliability of the air-bearing, especially the nature of the heat transfer mechanism [11], which may be enhanced due to the rarefied flow of particles. Further, it suggests that smear may travel unhindered by the moving gas in the head-disk spacing of HAMR drives as suggested in Ref. [46].

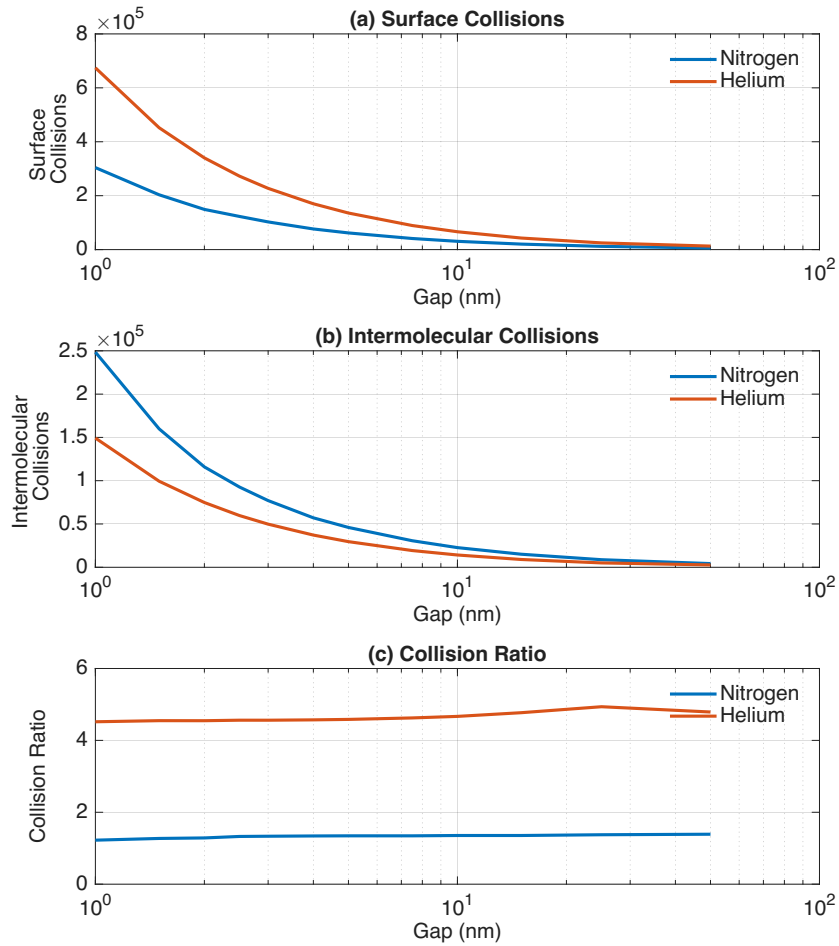


Fig. 9. The collision counts at the gap (which is the downtrack position of  $8 \mu\text{m}$  and  $10 \mu\text{m}$  in Fig. 3 (a) The surface collisions per timestep. (b) The intermolecular collisions per timestep. (c) The collision ratio (defined as the ratio between the surface and intermolecular collisions)

#### IV. CONCLUSION AND SCOPE FOR FUTURE WORK

In this study, we used the DSMC method to study the gas bearings of HAMR hard disk drives. We first modified the method by using the consistent Boltzmann algorithm to account for the dense gas effects. The stable nature of the DSMC approach provides a convenient method for simulating the air and material flow under the head-disk interface without concern for numerical errors and instabilities. The key results are summarized below:

- 1) The gas in nanometer level spacing is dominated by rarefied flow which implies

- a) The gas temperatures at the head and disk surfaces are not equal to those at the surfaces but are closer to the average of both surfaces.
  - b) The gas has a non-zero vertical component of velocity from the colder to the hotter surface. Further a positive vertical velocity overshoot is observed near the trailing edge that may trigger smear transport to the head surface.
  - c) The gas density in the air bearing is higher near the colder surface.
  - d) The gas molecules collide with the head and disk surfaces more often than with other molecules in the air bearing.
- 2) The partial pressure of the water vapor in the minimum spacing region exceeds the ambient partial pressure. The high saturation pressure at the higher head-disk interface prevents condensation from occurring. A future study that includes water evaporation from the disk would be expected to give a comprehensive understanding of humidity in the head-disk interface.

Future studies can also use the DSMC method to understand the impact these environmental conditions have on smear transport. We can start with the assumption that smear behaves like a granular gas [47, 48] in the head-disk interface. That way, smear can be added to the simulation as an additional gas (in addition to the helium, nitrogen, and water molecules). The DSMC code here, SPARTA, offers the ability to simulate chemical reactions ([49]), which can be utilized to study the decomposition/evaporation of the lubricant molecules. Subsequently, the kinetics of the decomposed smear molecules can be utilized to calculate the smear formation rate and other relevant quantities.

The collision model used in the current study assumes a variable soft sphere model which does not take into account the full range of intermolecular force. However, since smear consists of many kinds of materials, including metallic and organic molecules, the intermolecular forces will play a significant role. Therefore, a Lennard-Jones interaction model of Ref. [50] could be used instead of the variable soft sphere interaction model used in this study. An additional advantage of the DSMC method is that one can couple other kinds of mechanisms such as the optical force [4] in the head-disk interface. The advection step of Eq 6 can be modified to include the acceleration due to the external field. This coupling will allow us to study the interaction between forces such as air shear, optical force, and van der Waals forces on the smear molecules in the head-disk interface.

#### ACKNOWLEDGMENT

We thank Prof. Alejandro Garcia of San Jose State University for helpful discussions and the developers of SPARTA for guidance in modifying the tool. The Computer Mechanics Lab at UC Berkeley supported this work.

#### CONFLICT OF INTEREST

The authors declare no conflict of interest.

#### REFERENCES

- [1] Steven Granz et al. “Heat Assisted Magnetic Recording Areal Density Dependence on Writer Current for Conventional and Shingled Magnetic Recording”. In: *2023 IEEE 34th Magnetic Recording Conference (TMRC)*. IEEE. 2023, pp. 1–2.
- [2] Qilong Cheng and David B Bogy. “Experimental study of smear formation and removal in heat-assisted magnetic recording”. In: *Tribology International* 165 (2022), p. 107258.
- [3] Shaomin Xiong et al. “Material Transfer From Media to Head in Heat Assisted Magnetic Recording (HAMR)”. In: *Information Storage and Processing Systems*. Vol. 84799. American Society of Mechanical Engineers. 2021, V001T05A003.
- [4] Roshan Mathew Tom et al. “Optical forces in heat-assisted magnetic recording head-disk interface”. In: *Scientific Reports* 13.1 (2023), p. 8451.
- [5] Roshan Mathew Tom, Qilong Cheng, and David B Bogy. “A Numerical Simulation of PFPE Lubricant Kinetics in HAMR Air Bearing”. In: *Tribology Letters* 72.2 (2024), pp. 1–11.
- [6] Hiroshi Tani et al. “Effect of Humidity on Head Smear Generation in Head-Assisted Magnetic Recording”. In: *IEEE Transactions on Magnetics* 59.11 (2023), pp. 1–5.
- [7] Xingyu Chen et al. “Effect of water on mechano-chemical reactions of perfluoropolyether lubricant films in heat-assisted magnetic recording: A reactive molecular dynamics study”. In: *Tribology International* 187 (2023), p. 108674.
- [8] Kyosuke Ono. “Physics of the Sub-Monolayer Lubricant in the Head-Disk Interface”. In: *Lubricants* 12.4 (2024), p. 117.
- [9] Siddhesh V Sakhalkar and David B Bogy. “Effect of rheology and slip on lubricant deformation and disk-to-head transfer during heat-assisted magnetic recording (HAMR)”. In: *Tribology Letters* 66 (2018), pp. 1–19.
- [10] Qilong Cheng, Roshan Mathew Tom, and David B Bogy. “Two strategies to mitigate thermally-induced material buildup in heat-assisted magnetic recording”. In: *Tribology Letters* 71.2 (2023), p. 50.
- [11] S Sakhalkar et al. “Numerical and experimental investigation of heat transfer across a nanoscale gap between a magnetic recording head and various media”. In: *Applied Physics Letters* 115.22 (2019).
- [12] Hiroshi Tani et al. “Investigation of mechanism of smear formation from diamond-like carbon films on heating”. In: *Microsystem Technologies* 27 (2021), pp. 2243–2255.

- [13] Qingkang Liu et al. “Study on the thermal decomposition of d-4oh PFPE lubricant by reactive molecular dynamic simulation for HAMR”. In: *IEEE Transactions on Magnetics* 59.3 (2022), pp. 1–7.
- [14] Siddhesh V Sakhalkar and David B Bogy. “A model for lubricant transfer from media to head during heat-assisted magnetic recording (HAMR) writing”. In: *Tribology Letters* 65 (2017), pp. 1–15.
- [15] S. Fukui and R. Kaneko. “Analysis of Ultra-Thin Gas Film Lubrication Based on Linearized Boltzmann Equation: First Report—Derivation of a Generalized Lubrication Equation Including Thermal Creep Flow”. In: *Journal of Tribology* 110.2 (Apr. 1988), pp. 253–261. ISSN: 1528-8897.
- [16] Weidong Huang, David B Bogy, and Alejandro L Garcia. “Three-dimensional direct simulation Monte Carlo method for slider air bearings”. In: *Physics of Fluids* 9.6 (1997), pp. 1764–1769.
- [17] Qilong Cheng, Yuan Ma, and David Bogy. “Effect of Humidity on the Nanoscale Heat Transfer at the Head-Media Interface”. In: *ASME 2019 28th Conference on Information Storage and Processing Systems* (June 2019). DOI: 10.1115/isp2019-7449. URL: <http://dx.doi.org/10.1115/ISPS2019-7449>.
- [18] Nisha Shukla et al. “Effect of Humidity on Lubricated Carbon Overcoats”. In: *Tribology Letters* 12.2 (2002), pp. 105–109. DOI: 10.1023/a:1014085517456. URL: <https://doi.org/10.1023/A:1014085517456>.
- [19] Dae-Young Lee et al. “Effect of relative humidity and disk acceleration on tribocharge build-up at a slider–disk interface”. In: *Tribology International* 40.8 (Aug. 2007), pp. 1253–1257. DOI: 10.1016/j.triboint.2006.11.006. URL: <https://doi.org/10.1016/j.triboint.2006.11.006>.
- [20] Sang Hoon Kim et al. “Humidity effects on lubricant transfer in the head-disk interface of a hard disk drive”. In: *Journal of Applied Physics* 105.7 (2009). DOI: 10.1063/1.3061704.
- [21] Qilong Cheng et al. “Dependence of nanoscale heat transfer across a closing gap on the substrate material and ambient humidity”. In: *Applied Physics Letters* 116.21 (May 2020). DOI: 10.1063/5.0010286. URL: <https://doi.org/10.1063/5.0010286>.
- [22] Thomas E. Karis. “Water Adsorption on Thin Film Media”. In: *Journal of Colloid and Interface Science* 225.1 (May 2000), pp. 196–203. DOI: 10.1006/jcis.2000.6745. URL: <https://doi.org/10.1006/jcis.2000.6745>.
- [23] Ryan Z. Lei and Andrew J. Gellman. “Humidity Effects on PFPE Lubricant Bonding to a-CHx Overcoats”. In: *Langmuir* 16.16 (July 2000), pp. 6628–6635. DOI: 10.1021/la9915973. URL: <https://doi.org/10.1021/la9915973>.
- [24] G. W. Tyndall, R. J. Waltman, and J. Pacansky. “Effect of adsorbed water on perfluoropolyether-lubricated magnetic recording disks”. In: *Journal of Applied Physics* 90.12 (Dec. 2001), pp. 6287–6296. DOI: 10.1063/1.1413946. URL: <https://doi.org/10.1063/1.1413946>.
- [25] R. R. Dubin et al. “Degradation of Co-based thin-film recording materials in selected corrosive environments”. In: *Journal of Applied Physics* 53.3 (Mar. 1982), pp. 2579–2581. DOI: 10.1063/1.330913. URL: <https://doi.org/10.1063/1.330913>.
- [26] G A Bird. *Molecular gas dynamics and the direct simulation of gas flows*. en. Oxford Engineering Science Series. Oxford, England: Clarendon Press, May 1994.
- [27] Francis J Alexander, Alejandro L Garcia, et al. “The direct simulation Monte Carlo method”. In: *Computers in Physics* 11.6 (1997), p. 588.
- [28] GJ LeBeau. “A parallel implementation of the direct simulation Monte Carlo method”. In: *Computer methods in applied mechanics and engineering* 174.3-4 (1999), pp. 319–337.
- [29] Kenichi Nanbu. “Variable hard-sphere model for gas mixture”. In: *Journal of the Physical Society of Japan* 59.12 (1990), pp. 4331–4333.
- [30] Katsuhisa Koura and Hiroaki Matsumoto. “Variable soft sphere molecular model for inverse-power-law or Lennard-Jones potential”. In: *Physics of fluids A: fluid dynamics* 3.10 (1991), pp. 2459–2465.
- [31] HA Hassan and David B Hash. “A generalized hard-sphere model for Monte Carlo simulation”. In: *Physics of Fluids A: Fluid Dynamics* 5.3 (1993), pp. 738–744.
- [32] Andrew B. Weaver and Alina A. Alexeenko. “Revised Variable Soft Sphere and Lennard-Jones Model Parameters for Eight Common Gases up to 2200 K”. In: *Journal of Physical and Chemical Reference Data* 44.2 (June 2015). ISSN: 1529-7845. DOI: 10.1063/1.4921245. URL: <http://dx.doi.org/10.1063/1.4921245>.
- [33] Francis J Alexander, Alejandro L Garcia, and Berni J Alder. “Direct simulation Monte Carlo for thin-film bearings”. In: *Physics of Fluids* 6.12 (1994), pp. 3854–3860.
- [34] Shigehisa Fukui and Kiyomi Yamane. “DSMC/MGL comparisons of stresses on slider air bearing with nanometer spacings”. In: *IEEE transactions on magnetics* 38.5 (2002), pp. 2153–2155.
- [35] Alejandro L Garcia and Wolfgang Wagner. “The limiting kinetic equation of the consistent Boltzmann algorithm for dense gases”. In: *Journal of Statistical Physics* 101 (2000), pp. 1065–1086.
- [36] Johannes Diderik Van der Waals. *Over de Continuïteit van den Gas-en Vloeistoftoestand*. Vol. 1. Sijthoff, 1873.
- [37] Francis J Alexander, Alejandro L Garcia, and Berni J Alder. “A consistent Boltzmann algorithm”. In: *Physical Review Letters* 74.26 (1995), p. 5212.
- [38] JJ Brey et al. *25 Years of Non-Equilibrium Statistical Mechanics*. Springer, 1995.
- [39] Wolfgang Wagner. “A convergence proof for Bird’s direct simulation Monte Carlo method for the Boltzmann equation”. In: *Journal of Statistical Physics* 66 (1992), pp. 1011–1044.

- [40] E P Muntz. “Rarefied Gas Dynamics”. In: *Annual Review of Fluid Mechanics* 21.1 (Jan. 1989), pp. 387–422. ISSN: 1545-4479. DOI: 10.1146/annurev.fl.21.010189.002131. URL: <http://dx.doi.org/10.1146/annurev.fl.21.010189.002131>.
- [41] Roshan Mathew Tom and David B Bogy. “The Use of DSMC in HAMR Head-Disk Interface to Study Smear”. In: *2024 IEEE 35th Magnetic Recording Conference (TMRC)*. IEEE. 2024.
- [42] Steve J Plimpton et al. “Direct simulation Monte Carlo on petaflop supercomputers and beyond”. In: *Physics of Fluids* 31.8 (2019). URL: <http://sparta.sandia.gov>.
- [43] Roshan Mathew Tom. “A Particle-Level Study of Smear Buildup in Heat-Assisted Magnetic Recording Disk Drives”. Chapter 6. PhD thesis. Berkeley, CA: University of California, Berkeley, 2024.
- [44] P. L. Kapitza. “Heat Transfer and Superfluidity of Helium II”. In: *Physical Review* 60.4 (Aug. 1941), pp. 354–355. ISSN: 0031-899X. DOI: 10.1103/physrev.60.354. URL: <http://dx.doi.org/10.1103/PhysRev.60.354>.
- [45] Gerald L Pollack. “Kapitza resistance”. In: *Reviews of modern physics* 41.1 (1969), p. 48.
- [46] Roshan Mathew Tom and David B Bogy. “Ballistic material transport in HAMR head-disk interface”. In: *2023 IEEE 34th Magnetic Recording Conference (TMRC)*. IEEE. 2023, pp. 1–2.
- [47] Nikolai V. Brilliantov and Thorsten Pöschel. *Kinetic Theory of Granular Gases*. Oxford University Press, July 2004. ISBN: 9780198530381. DOI: 10.1093/acprof:oso/9780198530381.001.0001. URL: <https://doi.org/10.1093/acprof:oso/9780198530381.001.0001>.
- [48] Andrew Hong. “Direct Simulation Monte Carlo and Granular Gases”. In: (July 2022). DOI: 10.25394/PGS.20394291.v1. URL: [https://hammer.purdue.edu/articles/thesis/Direct\\_Simulation\\_Monte\\_Carlo\\_and\\_Granular\\_Gases/20394291](https://hammer.purdue.edu/articles/thesis/Direct_Simulation_Monte_Carlo_and_Granular_Gases/20394291).
- [49] S F Gimelshein et al. “On the use of chemical reaction rates with discrete internal energies in the direct simulation Monte Carlo method”. en. In: *Phys. Fluids (1994)* 16.7 (July 2004), pp. 2442–2451.
- [50] Ayyaswamy Venkatraman and Alina A Alexeenko. “Binary scattering model for Lennard-Jones potential: Transport coefficients and collision integrals for non-equilibrium gas flow simulations”. In: *Physics of Fluids* 24.2 (2012).